Electronic properties of gated triangular graphene quantum dots: Magnetism, correlations, and geometrical effects

P. Potasz,[1,2] A. D. Güçlü,[1] A. Wójs,[2] and P. Hawrylak[1]

[1]*Institute for Microstructural Sciences, National Research Council of Canada, Ottawa, Ontario, K1A 0R6 Canada*

[2]*Institute of Physics, Wroclaw University of Technology, PL-50-370 Wroclaw, Poland*

(Received 9 December 2011; revised manuscript received 16 January 2012; published 27 February 2012)

We present a theory of electronic properties of gated triangular graphene quantum dots with zigzag edges as a function of size and carrier density. We focus on electronic correlations, spin, and geometrical effects using a combination of atomistic tight-binding, Hartree-Fock, and configuration interaction methods (TB + HF + CI), including long-range Coulomb interactions. The single-particle energy spectrum of triangular dots with zigzag edges exhibits a degenerate shell at the Fermi level with a degeneracy N_{edge} proportional to the edge size. We determine the effect of the electron-electron interactions on the ground state, the total spin, and the excitation spectrum as a function of a shell filling and the degeneracy of the shell using TB + HF + CI for $N_{\mathrm{edge}} < 12$ and approximate CI method for $N_{\mathrm{edge}} \geqslant 12$. For a half-filled neutral shell we find spin-polarized ground state for structures up to $N = 500$ atoms in agreement with previous *ab initio* and mean-field calculations and in agreement with Lieb's theorem for a Hubbard model on a bipartite lattice. Adding a single electron leads to the complete spin depolarization for $N_{\mathrm{edge}} \leqslant 9$. For larger structures, the spin depolarization is shown to occur at different filling factors. Away from half-fillings excess electrons(holes) are shown to form Wigner-like spin-polarized triangular molecules corresponding to large gaps in the excitation spectrum. The validity of conclusions is assessed by a comparison of results obtained from different levels of approximations. While for the charge-neutral system all methods give qualitatively similar results, away from the charge neutrality an inclusion of all Coulomb scattering terms is necessary to produce results presented here.

DOI: 10.1103/PhysRevB.85.075431 PACS number(s): 73.22.Pr, 75.75.−c, 81.05.ue

I. INTRODUCTION

Graphene is an atomically thick layer of carbon atoms arranged in a honeycomb lattice.[1–10] Due to its unique electronic properties and promising potential for applications, there is a growing research interest in graphene-based nanostructures.[10–12] Attempts at fabricating graphene nanostructures with well-defined shape and edge type have been reported starting from the graphene layer and using top-down techniques,[13–25] bottom-up techniques[26–30] starting from carbon-based molecules, as well as starting from graphane and removing hydrogen atoms using AFM tips.[31–34]

The work on graphene nanostructures is motivated by the expectation that finite-size effects significantly modify electronic properties of graphene. As a result of size quantization, an energy gap opens up, making graphene a semiconductor with a gap tunable from THz to UV. The energy gap can be tuned by changing not only the size but also the shape and the type of edge, allowing us to control the material's optical properties.[35–37] Two types of edges in graphene are of particular interest due to their stability: armchair and zigzag. For zigzag edges, edge states in the vicinity of the Fermi energy appear. This is related to breaking the sublattice symmetry between the two types of atoms in the unit cell of the graphene honeycomb lattice. The presence of edge states was predicted theoretically[4,35,38–46] and confirmed experimentally.[47–49] These edge states form a degenerate band in graphene ribbons[4,38–41] or can collapse to a degenerate shell in graphene quantum dots.[35,42–46,50,51] It was previously shown that the degeneracy is equal to the difference between the number of atoms corresponding to two sublattices in the bipartite lattice.[42,43,46,50] In particular, the geometry that maximizes the imbalance between the two sublattices is a zigzag edge triangle where the degeneracy of the zero-energy shell is proportional to the number of atoms on the one edge.[46] This presents a unique opportunity to design a quantum system with a macroscopic degeneracy, analogously to the two-dimensional electron gas in a strong magnetic field.

While fabricating and measuring triangular graphene quantum dots with well-defined edges[20,26,29,30] remains a challenge, the theory of triangular graphene quantum dots (TGQD) with zigzag edges was developed by several groups.[29,35,37,42–44,46,50–64] In particular, the macroscopically degenerate zero-energy band and the corresponding wave functions were explicitely constructed.[46] For a half-filled shell, TGQDs were studied by Ezawa using the Heisenberg Hamiltonian;[42] by Fernandez-Rossier and Palacios[43] using the mean-field Hubbard model; by Wang, Meng, and Kaxiras[50] using density functional theory (DFT); and Güçlü *et al.*[51] using exact diagonalization techniques. It was shown that the ground state is fully spin polarized, with a finite magnetic moment proportional to the shell degeneracy. This finding is in agreement with Lieb's theorem on magnetism of the Hubbard model for bipartite lattice systems.[65]

The effect of defects and disorder was also investigated.[46,57,58] In particular, Voznyy *et al.*[58] have shown by using *ab initio* methods that hydrogen-passivation stabilizes zigzag edges in TGQD over the pentagon-heptagon reconstructed edges.[58] It was also proved that the zero-energy shell survives when TGQD is deformed to trapezoidal shape.[46] Ezawa studied the stability of magnetization against disorder. He considered three types of randomness: in a hopping integral, a site energy, and lattice defects.[57] He proved that the magnetism is still governed by Lieb's theorem but the

number of degenerate states changed by the number of lattice defects. Some of us have shown in Ref. 51, by use of methods beyond mean-field approximations, that the magnetization is unstable with respect to additional charge, leading to a complete spin depolarization. The spin depolarization was shown to significantly influence transport properties, blocking current through the graphene quantum dot due to the spin blockade.[51] It was also shown that by changing the population of the degenerate shell using a gate, one can simultaneously control magnetic and optical properties, determined by strong electron-electron and excitonic interactions.[37]

In this work we use improved configuration-interaction (CI) tools to extend our previous results[51] regarding the role of electron-electron interactions, magnetism, and correlations in TGQDs to larger structures. We investigate the electronic properties as a function of size and filling factor of the degenerate shell by using a combination of tight-binding (TB), Hartree-Fock (HF), and configuration interaction methods (TB + HF + CI). Our many-body Hamiltonian includes, in addition to the on-site interaction term, all scattering and exchange terms within next-nearest neighbors and all direct interaction terms in the two-body Coulomb matrix elements. Using full CI combined with the TB + HF method we demonstrate that the ground state for the charge-neutral system has maximally polarized edge states for structures consisting of up to 200 atoms with the number of degenerate edge states $N_{\mathrm{edge}} \leqslant 9$. By analyzing a spin-flip excitation spectrum of the spin-polarized ground state, we verify the spin-polarized ground state for up to 500 atoms or $N_{\mathrm{edge}} = 20$. These results for a system with long-ranged Coulomb interaction appear to be consistent with Lieb's theorem for the Hubbard model. Using TB + HF + full CI method for TGQD charged with an additional electron and a size of up to $N = 200$ atoms it is shown that a complete spin depolarization predicted earlier by some of us[51] exists only up to a critical size. The critical size is established by studying the stability of a charged spin-polarized shell to spin-flip excitations. It is shown that for sizes up to the critical size the spin wave and minority spin electron form a bound state, a trion, signaling the tendency to the depolarization. For sizes exceeding the critical size the spin waves are unbound and the spin-polarized state is the ground state up to the sizes studied ($N \approx 500$ atoms). For TGQD structures above the critical size, depolarization effects away from the half-filling are observed. Results of TB + HF + CI calculations allow us to extract the excitation gap as a function of a shell filling. It is found that the largest gaps correspond to the half-filled spin-polarized shell and special filling fractions. At these special filling fractions, we predict a formation of Wigner-like spin-polarized molecules, related to long-range Coulomb interactions and a triangular geometry of graphene quantum dot. Finally, we compare results obtained at different levels of approximations. We show that, for the charge-neutral system, the Hubbard, extended Hubbard, and fully interacting models are in good qualitative agreement. On the other hand, away from the half-filling, only a fully interacting model is able to correctly capture the effect of correlations.

The paper is organized as follows. In Sec. II, we describe our model. Section III contains analysis of the ground-state spin and correlations as a function of size and filling factor of the degenerate shell. In Sec. IV, we compare results obtained within different levels of approximations. In Sec. V, we summarize our results.

II. MODEL OF A GRAPHENE TRIANGULAR QUANTUM DOT

Graphene is a two-dimensional honeycomb crystal formed by carbon atoms on two interpenetrating hexagonal sublattices. The unit cell thus contains two carbon atoms. The distance between nearest-neighbor atoms is $a = 1.42$ Å. By using vectors $\mathbf{R} = n\mathbf{a}_1 + m\mathbf{a}_2$ with n,m integers and primitive unit vectors defined as $\mathbf{a}_{1,2} = a/2(\pm\sqrt{3},3)$, one can obtain the positions of all the atoms in the structure. By cutting the graphene lattice in three zigzag directions, an equilateral triangle can be obtained, as shown in Fig. 1. Such a system has a broken sublattice symmetry with two properties: (i) all edge atoms (with only two bonds) belong to the same sublattice and (ii) the difference between the number of atoms belonging to each sublattice is proportional to the number of atoms on one of the three edges.

Each carbon atom has four valence electrons. Three of them, on s, p_x, and p_y orbitals, form sp^2 bonds with the three nearest in-plane neighbors. They are strongly bound and responsible for mechanical properties of graphene. The remaining fourth valence electron on each carbon atom p_z orbital, perpendicular to the plane of graphene, is weakly bound and determines electronic properties of the system. Single-particle properties of graphene can be described by using one orbital tight-binding (TB) Hamiltonian.[66] We have previously shown that, within the TB model in the nearest-neighbors approximation, TGQDs with zigzag edges exhibit an energy gap, with a degenerate shell at the Fermi (zero) energy, with a degeneracy proportional to the length of an edge.[46] An example of TB energy levels for a structure consisting of 97 atoms with $N_{\mathrm{edge}} = 7$ degenerate states is shown in Fig. 2(a). Our goal is to study the role of electron-electron interactions for electrons occupying this degenerate shell. Solving the full many-body

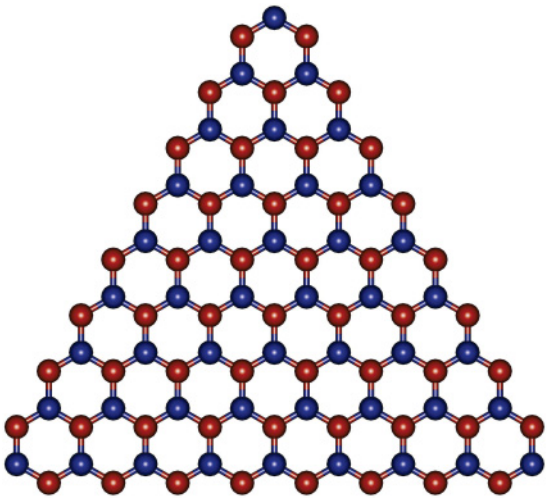

FIG. 1. (Color online) Triangular graphene quantum dot with zigzag edges. There are eight edge atoms (with two bonds) on one edge. Red (light gray) and blue (dark gray) colors distinguish between two sublattices in the honeycomb graphene lattice. Structure consists of a total of $N = 97$ atoms

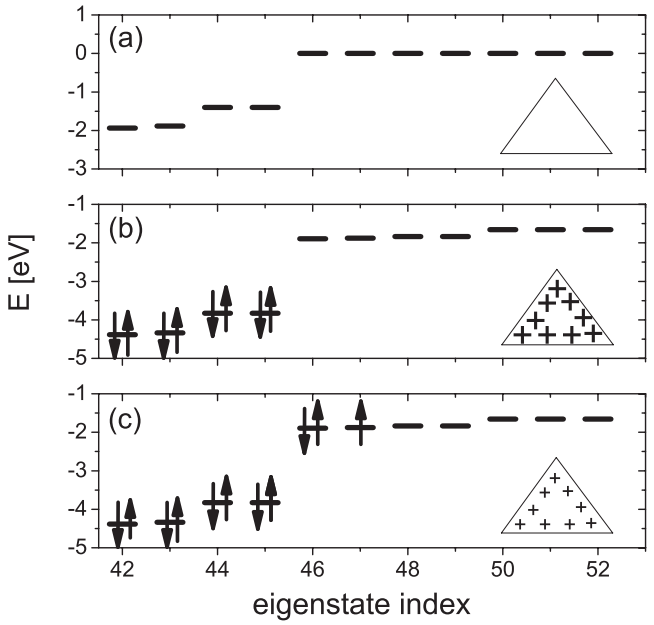

FIG. 2. (a) Single-particle nearest-neighbor tight-binding (TB) energy levels. The zero-energy shell on the Fermi level is perfectly degenerate. (b) Positively charged system with an empty degenerate band after self-consistent Hartee-Fock (HF) mean-field calculations described by a single Slater determinant (TB + HF model). (c) Occupation of empty degenerate HF quasiorbitals by electrons. The inset pictures schematically show the excess charge corresponding to each of the three model systems. The ground state and the total spin of the system of interacting electrons can be calculated by using the configuration interaction (CI) method, described in Sec. II (TB + HF + CI). The charge neutrality corresponds to a half-filled degenerate band (not shown).

problem even for such a small structure with 97 atoms is not possible at present. However, due to the energy gap separating the valence band and degenerate states, the valence electrons that do not occupy the degenerate band can be treated in a mean-field approximation. The remaining electrons occupying the degenerate shell must, however, be treated using a configuration-interaction method (CI). Therefore, we use a TB + HF + CI approach that allows us to treat the electronic correlations for electrons in the degenerate shell and their interaction with valence electrons at the mean-field level.

We start from the full many-body Hamiltonian for interacting electrons on the p_z orbitals of graphene. It can be written as

$$H = \sum_{i,l,\sigma} \tau_{il\sigma} c^\dagger_{i\sigma} c_{l\sigma} + \frac{1}{2} \sum_{\substack{i,j,k,l,\\ \sigma\sigma'}} \langle ij|V|kl\rangle c^\dagger_{i\sigma} c^\dagger_{j\sigma'} c_{k\sigma'} c_{l\sigma}, \quad (1)$$

where the operator $c^\dagger_{i\sigma}$ creates an electron on the i-th p_z orbital with spin σ, $\tau_{il\sigma}$ is a hopping integral that describes the probability of scattering of electron on the l-th p_z orbital ϕ_l to the i-th p_z orbital ϕ_i. The second term describes two-body Coulomb interactions between p_z electrons. Note that, at this stage, the unknown hopping terms $\tau_{il\sigma}$ do not include the effect of electron-electron interactions of p_z electrons.

A. Mean-field approximation for infinite graphene sheet

Let us, first, write the Hamiltonian for graphene, given by Eq. (1), in the mean-field Hartree-Fock (HF) approximation as

$$H^o_{\rm MF} = \sum_{i,l,\sigma} \tau_{il\sigma} c^\dagger_{i\sigma} c_{l\sigma} + \sum_{i,l,\sigma} \sum_{j,k,\sigma'} \rho^o_{jk\sigma'} (\langle ij|V|kl\rangle - \langle ij|V|lk\rangle \delta_{\sigma,\sigma'}) c^\dagger_{i\sigma} c_{l\sigma} = \sum_{i,l,\sigma} t_{il\sigma} c^\dagger_{i\sigma} c_{l\sigma}. \quad (2)$$

This is effectively a one-body TB Hamiltonian for a graphene layer[66] with density matrix elements $\rho^o_{jk\sigma'} = \langle c^\dagger_{j\sigma'} c_{k\sigma'}\rangle$ calculated with respect to the fully occupied valence band. The values of $\rho^o_{jk\sigma'}$ are evaluated in Appendix and their role becomes clear in the next subsection. $t_{il\sigma}$ are experimentally estimated hopping integrals.

B. Mean-field approximation for graphene quantum dots

We now derive a mean-field Hamiltonian for electrons in graphene quantum dots (GQD). First, we apply mean-field approximation to the Hamiltonian given by Eq. (1) for electrons in GQD, with a result written as

$$H^{\rm GQD}_{\rm MF} = \sum_{i,l,\sigma} \tau_{il\sigma} c^\dagger_{i\sigma} c_{l\sigma} + \sum_{i,l,\sigma} \sum_{j,k,\sigma'} \rho_{jk\sigma'} (\langle ij|V|kl\rangle - \langle ij|V|lk\rangle \delta_{\sigma,\sigma'}) c^\dagger_{i\sigma} c_{l\sigma}, \quad (3)$$

with density matrix $\rho_{jk\sigma'}$ for GQD. By combining Eq. (2) and Eq. (3) we get

$$\begin{aligned} H^{\rm GQD}_{\rm MF} &= H^{\rm GQD}_{\rm MF} - H^o_{\rm MF} + H^o_{\rm MF} \\ &= \sum_{i,l,\sigma} t_{il\sigma} c^\dagger_{i\sigma} c_{l\sigma} + \sum_{i,l,\sigma} \sum_{j,k,\sigma'} \left(\rho_{jk\sigma'} - \rho^o_{jk\sigma'}\right) (\langle ij|V|kl\rangle - \langle ij|V|lk\rangle \delta_{\sigma,\sigma'}) c^\dagger_{i\sigma} c_{l\sigma}. \end{aligned} \quad (4)$$

Here the subtracted component in the second term corresponds to mean-field interactions included in effective $t_{il\sigma}$ hopping integrals, described by the graphene density matrix $\rho^o_{jk\sigma'}$. For the TGQDs, the density matrix elements $\rho_{jk\sigma'}$ are calculated with respect to the many-body ground state of $N_{\rm ref} = N_{\rm site} - N_{\rm edge}$ electrons, where $N_{\rm site}$ is the number of atoms. Since the valence band and the degenerate shell are separated by an energy gap, the closed-shell system of $N_{\rm ref}$ interacting electrons is expected to be well described in a mean-field approximation, using a single Slater determinant. This corresponds to a charged system with $N_{\rm edge}$ positive charges, as schematically shown in Fig. 2(b). The Hamiltonian given by Eq. (4) has to be solved self-consistently to obtain Hartree-Fock quasiparticle orbitals. In numerical calculations, in addition to the on-site interaction term, all scattering and exchange terms within next-nearest neighbors and all direct interaction terms are included in the two-body Coulomb matrix elements $\langle ij|V|kl\rangle$ computed using Slater p_z orbitals.[67] The few largest Coulomb matrix elements are given in Ref. 68. The value of the effective dielectric constant κ depends on the substrate and is set to $\kappa = 6$ in what follows.[69] A method of calculating values of $\rho^o_{jk\sigma'}$ for graphene is shown in Appendix. Values of hopping integrals $t_{il\sigma}$ are taken from the experimental data[70] or *ab initio* calculation.[69] We use $t = -2.5$ eV for nearest-neighbors and $t' = -0.1$ eV for next-nearest-neighbors[71] hopping matrix elements. The

HF results were also compared with the results of *ab initio* calculations.[51,58]

We now discuss mean-field results for the charge-neutral system. In the vicinity of the center of a sufficiently large dot a charge distribution around a given site is identical to that of an infinite system. The density matrices for graphene $\rho^o_{jk\sigma'}$ and for GQD $\rho_{jk\sigma'}$ are equal. A second term in Eq. (4) vanishes, leaving only a hopping integral $t_{il\sigma}$. On the other hand, close to the edges, a density matrix for the GQD differs in comparison to its graphene counterpart. After diagonalizing the HF Hamiltonian given by Eq. (4) one obtains eigenvalues and eigenvectors that involve the geometrical properties of the system, shown in Fig. 2(b). A slight removal of the degeneracy of middle edge states and three corner states with a bit higher energies are observed, with electronic densities shown in Ref. 51.

C. Configuration interaction method

After the self-consistent procedure we get new orbitals for quasiparticles with a fully occupied valence band and a completely empty degenerate shell. We start filling these degenerate states by adding extra electrons one by one, schematically shown in Fig. 2(c). Next, we solve the many-body Hamiltonian corresponding to the added electrons, given by

$$H_{\mathrm{MB}} = \sum_{s,\sigma} \epsilon_s a^\dagger_{s\sigma} a_{s\sigma} + \frac{1}{2} \sum_{\substack{s,p,d,f,\\ \sigma,\sigma'}} \langle sp|V|df\rangle a^\dagger_{s\sigma} a^\dagger_{p\sigma'} a_{d\sigma'} a_{f\sigma}, \tag{5}$$

where the first term describes the energies of the Hartree-Fock orbitals and the second term describes an interaction between quasiparticles occupying degenerate HF states denoted by s,p,d,f indices. The two-body quasiparticle scattering matrix elements $\langle sp|V|df\rangle$ are calculated from the two-body localized on-site Coulomb matrix elements $\langle ij|V|kl\rangle$.

In our calculations, we neglect scattering from/to the states from a fully occupied valence band. Moreover, because of the large energy gap between the shell and the conduction band, we can neglect scatterings to the higher energy states. A validity of these approximations is assessed in Ref. 68. These approximations allow us to treat the degenerate shell as an independent system that significantly reduces the dimension of the Hilbert space. The basis is constructed from vectors corresponding to all possible many-body configurations of electrons distributed within the degenerate shell. For a given number of electrons N_{el}, the Hamiltonian given by Eq. (5) is diagonalized in each subspace with total S_z.

D. Effect of gate charge

In our model, we start from the system with an empty shell that corresponds to the charged system. As in our previous work, Ref. 51, electrons from the shell are transferred to the metallic gate. The Hamiltonian for N_{ref} electrons in the presence of a gate in the mean-field Hartree-Fock approximation was written as

$$H_{\mathrm{MF}} = \sum_{i,l,\sigma} t_{il\sigma} c^\dagger_{i\sigma} c_{l\sigma} + \sum_{i,l,\sigma} \sum_{j,k,\sigma'} \left(\rho_{jk\sigma'} - \rho^o_{jk\sigma'}\right)\left(\langle ij|V|kl\rangle - \langle ij|V|lk\rangle \delta_{\sigma,\sigma'}\right) c^\dagger_{i\sigma} c_{l\sigma} + \sum_{i,\sigma} v^g_{ii}(q_{\mathrm{ind}}) c^\dagger_{i\sigma} c_{i\sigma}, \tag{6}$$

with an electrostatic potential v^g_{ii} related to N_{edge} electrons in a gate defined as

$$v^g_{ii}(q_{\mathrm{ind}}) = \sum_{j=1}^{N_{\mathrm{site}}} \frac{-q_{\mathrm{ind}}/N_{\mathrm{site}}}{\kappa\sqrt{(x_i - x_j)^2 + (y_i - y_j)^2 + d^2_{\mathrm{gate}}}} \tag{7}$$

with $q_{\mathrm{ind}} = -N_{\mathrm{edge}}$ charge smeared out at positions (x_i, y_i) at a distance d_{gate} from the quantum dot. Next, we derived the many-body Hamiltonian with an inclusion of the effect of gate, written as

$$H = \sum_{p,\sigma} \epsilon_p a^\dagger_{p\sigma} a_{p\sigma} + \frac{1}{2} \sum_{\substack{p,q,r,s,\\ \sigma,\sigma'}} \langle pq|V|rs\rangle a^\dagger_{p\sigma} a^\dagger_{q\sigma'} a_{r\sigma'} a_{s\sigma} + \sum_{p,q,\sigma} \langle p|v^g(N_{\mathrm{add}})|q\rangle a^\dagger_{p\sigma} a_{q\sigma} + 2\sum_{p'} \langle p'|v^g(N_{\mathrm{add}})|p'\rangle, \tag{8}$$

where the indices without the prime sign (p,q,r,s) run over N_{edge} degenerate states, while the index with the prime sign p' runs over $N_{\mathrm{ref}}/2$ valence states (below the degenerate shell). A third term in Eq. (8) corresponds to scattering from state q to state p in a degenerate shell as a result of interactions with electrons in a gate. The fourth term is a constant and just shifts the entire spectrum by a constant energy.

III. MAGNETISM AND CORRELATION EFFECTS

A. Electronic properties as a function of the filling factor

We, first, concentrate on a TGQD consisting of $N = 97$ atoms, which is the largest system previously studied in our earlier work in Ref. 51. It has $N_{\mathrm{edge}} = 7$ zero-energy degenerate states obtained from TB calculations, shown in Fig. 2(a). After self-consistent HF calculations neglecting the gate charge (the effect of the gate will be discussed later), we obtain new quasiparticle orbitals, shown in Fig. 2(b). The degeneracy is slightly removed. We fill these degenerate levels by additional electrons and calculate two-body scattering matrix elements. For a given number of quasiparticles, the many-body Hamiltonian, Eq. (5), is diagonalized in a basis of configurations of electrons distributed within the shell, as explained in Sec. II. In Fig. 3, we analyze the dependence of the low-energy spectra on the total spin S for [Fig. 3(a)] the charge-neutral system, $N_{\mathrm{el}} = 7$ electrons and [Fig. 3(b)] one added electron, i.e., $N_{\mathrm{el}} = 8$ electrons. We see that for the charge-neutral TGQD with $N_{\mathrm{el}} = 7$ electrons the ground state of the system is maximally spin polarized, with $S = 3.5$, indicated by a circle. There is only one possible configuration of all electrons with parallel spins that corresponds to exactly one electron per one degenerate state. The energy of this configuration is well separated from other states with lower total spin S, which require at least one flipped spin among

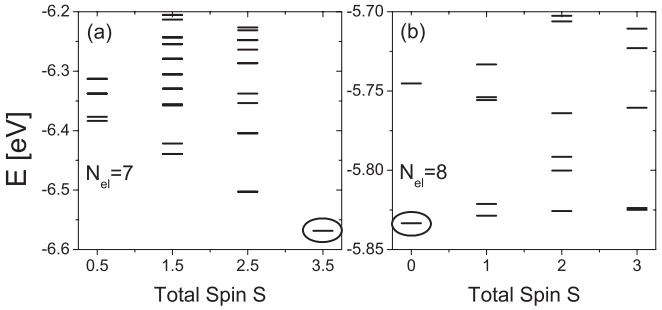

FIG. 3. The low-energy spectra for the different total spin S for (a) $N_{el} = 7$ electrons and (b) $N_{el} = 8$ electrons. For $N_{el} = 7$ electrons the ground state corresponding to $S = 3.5$, indicated by a circle, is well separated from excited states with different total spin S. For $N_{el} = 8$ electrons the ground state corresponding to $S = 0$, indicated by a circle, is almost degenerate with excited states with different total spin S.

seven initially spin-polarized electrons. An addition of one extra electron to the system with $N_{el} = 7$ spin-polarized electrons induces correlations as seen in Fig. 3(b), where the cost of flipping one spin is very small. Moreover, for $N_{el} = 8$, the ground state is completely depolarized with $S = 0$, indicated by a circle, but this ground state is almost degenerate with states corresponding to the different total spin.

The calculated many-body energy levels, including all spin states for different numbers of electrons (shell filling), are shown in Fig. 4. For each electron number, N_{el}, energies are measured from the ground-state energy and scaled by the energy gap of the half-filled shell, corresponding to $N_{el} = 7$ electrons in this case. The solid line shows the evolution of the energy gap as a function of shell filling. The energy gaps for a neutral system, $N_{el} = 7$, as well as for $N_{el} = 7 - 3 = 4$

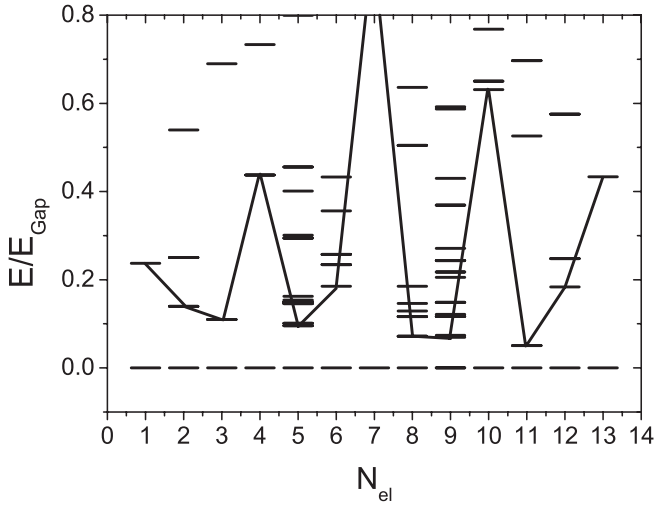

FIG. 4. The low-energy spectra of the many-body states as a function of the number of electrons occupying the degenerate shell for the system with $N_{edge} = 7$ degenerate states. The energies are renormalized by the energy gap corresponding to the half-filled shell, $N_{el} = 7$ electrons. A large density of states around $N_{edge} + 1$ electrons is a signature of the correlation effects. The solid line shows the evolution of the energy gap as a function of shell filling.

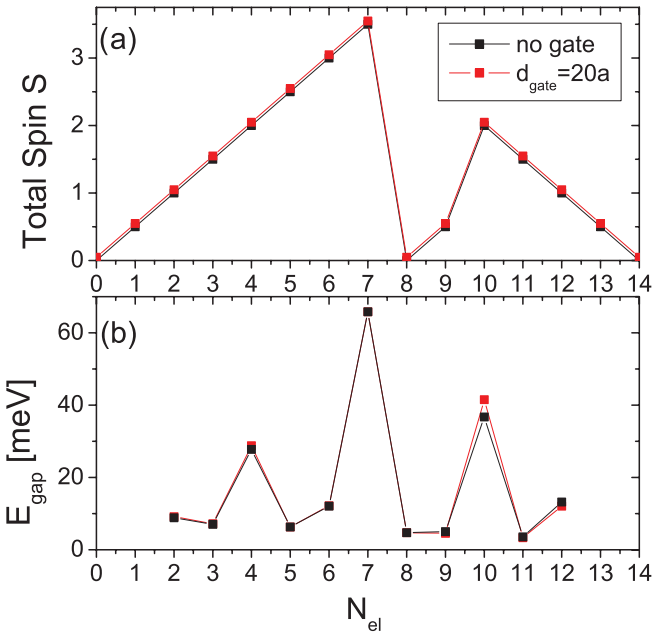

FIG. 5. (Color online) (a) The total spin as a function of number of electrons occupying the degenerate shell and (b) corresponding the energy excitation gaps, with and without a gate, red (light gray) and black (dark gray) lines, respectively. Due to a presence of correlation effects for some fillings, the magnitude of the energy gap is significantly reduced.

and $N_{el} = 7 + 3 = 10$, are found to be significantly larger in comparison to the energy gaps for other electron numbers. In addition, close to the half-filled degenerate shell, the reduction of the energy gap is accompanied by an increase of low-energy density of states. This is a signature of correlation effects, showing that they can play an important role at different filling factors.

We now extract the total spin and energy gap for each electron number. Figures 5(a) and 5(b) show the phase diagram, the total spin S, and an excitation gap as a function of the number of electrons occupying the degenerate shell. The system reveals maximal spin polarization for almost all fillings, with exceptions for $N_{el} = 8,9$ electrons. However, the energy gaps are found to strongly oscillate as a function of shell filling as a result of a combined effect of correlations and system's geometry. We observe a competition between fully spin-polarized system that maximizes exchange energy and fully unpolarized system that maximizes the correlation energy. Only close to the charge neutrality, for $N_{el} = 8$ and $N_{el} = 9$ electrons, are the correlations sufficiently strong to overcome the large cost of the exchange energy related to flipping spin. The excitation gap is significantly reduced and exhibits large density of states at low energies, as shown in Fig. 3.

Away from half-filling, we observe larger excitation gaps for $N_{el} = 4$ and $N_{el} = 10$ electrons. These fillings correspond to subtracting/adding three electrons from/to the charge-neutral system with $N_{el} = 7$ electrons. In Fig. 6 we show the corresponding spin densities. Here, long-range interactions dominate the physics and three spin-polarized [Fig. 6(a)] holes

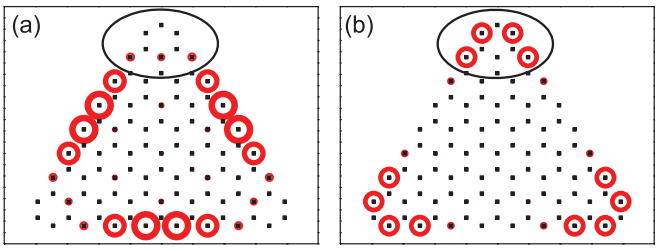

FIG. 6. (Color online) The spin densities of the ground state for (a) $N_{\rm el} = 4$ electrons and (b) $N_{\rm el} = 10$ electrons that correspond to subtracting/adding three electrons from/to the charge-neutral system. The radius of circles is proportional to a value of spin density on a given atom. A long-range Coulomb interaction repels (a) holes and (b) electrons to three corners, forming a spin-polarized Wigner-like molecule.

($N_{\rm el} = 7 - 3$ electrons) and [Fig. 6(b)] electrons ($N_{\rm el} = 7 + 3$ electrons) maximize their relative distance by occupying three consecutive corners. Electron spin density is localized in each corner while holes correspond to missing spin density localized in each corner. We also note that this is not observed for $N_{\rm el} = 3$ electrons filling the degenerate shell (not shown here). The energies of HF orbitals of corner states correspond to three higher energy levels [see Fig. 12(c)], with electronic densities shown in Ref. 51. Thus, $N_{\rm el} = 3$ electrons occupy lower-energy degenerate levels corresponding to sides instead of corners. On the other hand, when $N_{\rm el} = 7$ electrons are added to the shell, self-energies of extra electrons renormalize the energies of HF orbitals. The degenerate shell is again almost perfectly flat, similarly to levels obtained within the TB model. A kinetic energy does not play a role allowing a formation of a spin-polarized Wigner-like molecule, resulting from a long-range interactions and a triangular geometry. We note that Wigner molecules were previously discussed in circular graphene quantum dots with zigzag edges described in the effective mass approximation.[72,73] The rotational symmetry of quantum dot allowed for the construction of an approximate correlated ground state corresponding to either a Wigner-crystal or Laughlin-like state.[72] Later, a variational rotating-electron-molecule (VREM) wave function was used.[73] Unfortunately, due to a lack of an analytical form of a correlated wave function with a triangular symmetry, it is not possible to do it here.

Figure 5 also shows the effect of the presence of a gate at a distance $d_{\rm gate} = 20a$, where $a = 1.42$ is a nearest-neighbor's interatomic distance. Clearly, the effect of a gate is very weak, just slightly changing energy gaps. In Fig. 7, energy gaps as a function of a gate distance for the charge-neutral $N_{\rm el} = 7$ and charged $N_{\rm el} = 8$ system for our tested system with $N_{\rm edge} = 7$ degenerate states are shown. There are no effects for a gate distance $d_{\rm gate} \geqslant 20a$. When a gate distance is comparable to graphene-substrate separation, $d_{\rm gate} \sim 5a$, the energy gap for $N_{\rm el} = 7$ increases while the energy gap for $N_{\rm el} = 8$ decreases. The drop for $N_{\rm el} = 8$ is not sufficiently strong to change an observed effect of the spin depolarization. According to the above analysis, we next present results for a Hamiltonian with a gate at infinity.

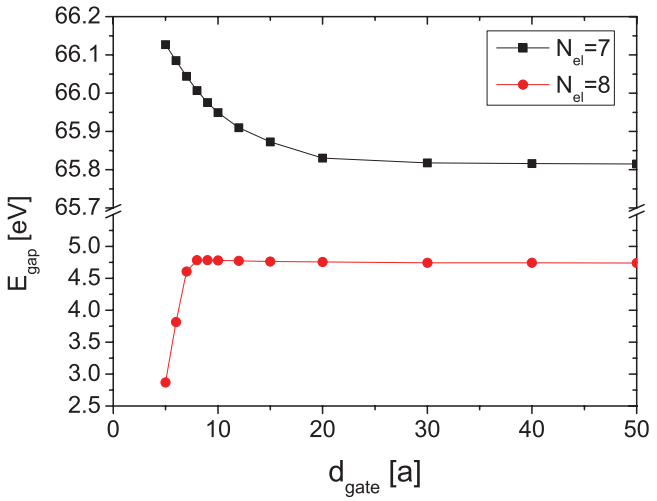

FIG. 7. (Color online) The energy gaps around the charge neutrality for a system with $N_{\rm edge} = 7$ degenerate states as a function of a gate distance. The energy gap for the charge-neutral system, $N_{\rm el} = 7$, changes by less than 1%. For the charged system, $N_{\rm el} = 8$, we observe changes in the energy gap for a gate distance in a range $5a \leqslant d_{\rm gate} \leqslant 10a$ but still not affecting the spin depolarization.

B. Electronic properties as a function of the size

In a previous section, we have analyzed in detail the electronic properties of a particular TGQD with $N = 97$ atoms as a function of the filling factor $\nu = N_{\rm el}/N_{\rm edge}$, i.e., the number of electrons per number of degenerate levels. In this section we address the important question of whether one can predict the electronic properties of a TGQD as a function of size.

Figure 8 shows spin phase diagrams for triangles with odd number of degenerate edge states $N_{\rm edge}$ and increasing size. Clearly, the total spin depends on the filling factor and size of the triangle. However, all charge-neutral systems at $\nu = 1$ are always maximally spin polarized and a complete depolarization occurs for $N_{\rm edge} \leqslant 9$ for structures with one extra electron added (such depolarization also occurs for even $N_{\rm edge}$, not shown). Similar results for small size triangles were obtained in our previous work.[51] However, at $N_{\rm edge} = 11$ we do not observe depolarization for $N_{\rm edge} + 1$ electrons but for $N_{\rm edge} + 3$, where a formation of Wigner-like molecule for a triangle with $N_{\rm edge} = 7$ was observed. We will come back to this problem later. We now focus on the properties close to the charge neutrality.

For the charge-neutral case, the ground state corresponds to only one configuration $|{\rm GS}\rangle = \prod_i a^\dagger_{i,\downarrow}|0\rangle$ with maximum total S_z and occupation of all degenerate shell levels i by electrons with parallel spin. Here $|0\rangle$ is the HF ground state of all valence electrons. Let us consider the stability of the spin-polarized state to single spin flips. We construct spin-flip excitations $|kl\rangle = a^\dagger_{k,\uparrow}a_{l,\downarrow}|{\rm GS}\rangle$ from the spin-polarized degenerate shell. The spin-up electron interacts with a spin-down "hole" in a spin-polarized state and forms a collective excitation, an exciton. An exciton spectrum is obtained by building an exciton Hamiltonian in the space of electron-hole pair excitations and diagonalizing it numerically, as was done, e.g., for quantum dots.[74] If the energy of the spin-flip excitation

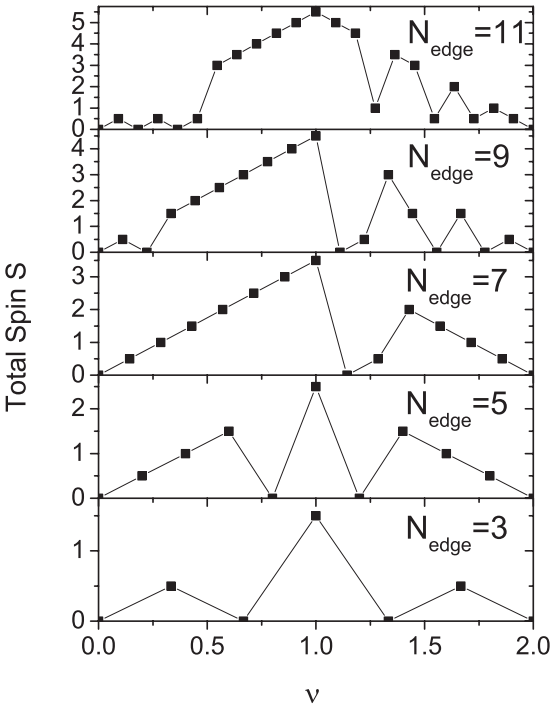

FIG. 8. Spin phase diagrams as a function of filling factor $\nu = N_{\rm el}/N_{\rm edge}$ for different size triangles characterized by the number of the degenerate edge states $N_{\rm edge}$. Half-filled shell $\nu = 1$ is always maximally spin polarized. The complete spin depolarization occurs for one added electron to the charge-neutral system for $N_{\rm edge} \leqslant 9$. For $N_{\rm edge} = 11$ the depolarization effect moves to a different filling.

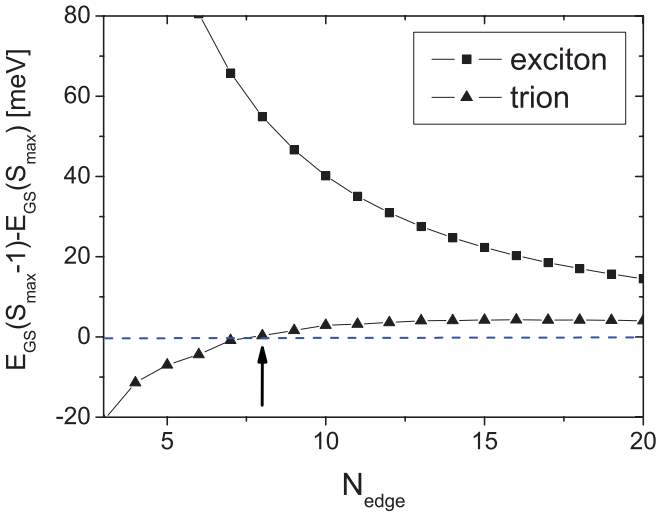

FIG. 9. Size-dependent analysis based on exciton and trion binding energies. For the charge-neutral system, it is energetically unfavorable to form an exciton, which is characterized by a positive binding energy. Observed dependence confirms Lieb's theorem regarding the magnetization of the bipartite lattice systems. The formation of a trion is desirable for small size systems. The phase transition occurs close to $N_{\rm edge} = 8$, indicated by an arrow. The complete depolarization effects close to the charge neutrality observed previously in TGQD with $N_{\rm edge} \leqslant 9$ for $N_{\rm edge} + 1$ electrons in Fig. 8 is predicted to not appear for larger systems.

turns out to be negative in comparison with the spin-polarized ground state, the exciton is bound and the spin-polarized state is unstable. The binding energy of a spin-flip exciton is a difference between the energy of the lowest state with $S = S_z^{\rm max} - 1$ and the energy of the spin-polarized ground state with $S = S_z^{\rm max}$. An advantage of this approach is the ability to test the stability of the spin-polarized ground state for much larger TGQD sizes.

Figure 9 shows the exciton binding energy as a function of the size of TGQD, labeled by a number of the degenerate states $N_{\rm edge}$. The largest system, with $N_{\rm edge} = 20$, corresponds to a structure consisting of $N = 526$ atoms. The exciton binding energies are always positive, i.e., the exciton does not form a bound state, confirming a stable magnetization of the charge-neutral system. The observed ferromagnetic order was also found by other groups based on calculations for small systems with different levels of approximations.[42,43,50,51] The above results confirm predictions based on Lieb's theorem for a Hubbard model on bipartite lattice relating total spin to the broken sublattice symmetry.[65] Unlike in Lieb's theorem, in our calculations many-body interacting Hamiltonian contains direct long-range, exchange, and scattering terms. Moreover, we include next-nearest-neighbor hopping integral in HF self-consistent calculations that slightly violates bipartite lattice property of the system, one of cornerstones of Lieb's arguments.[65] Nevertheless, the main result of the spin-polarized ground state for the charge-neutral TGQD seems to be consistent with predictions of Lieb's theorem and, hence, applicable to much larger systems.

Having established the spin polarization of the charge-neutral TGQD we now discuss the spin of charged TGQD. We start with a spin-polarized ground state $|{\rm GS}\rangle$ of a charge-neutral TGQD with all electron spins down and add to it a minority spin electron in any of the degenerate shell states i as $|i\rangle = a^\dagger_{i,\uparrow}|{\rm GS}\rangle$. The total spin of these states is $S_z^{\rm max} - 1/2$. We next study stability of such states with one minority spin-up electron to spin-flip excitations by forming three particle states $|lki\rangle = a^\dagger_{l,\uparrow}a_{k,\downarrow}a^\dagger_{i,\uparrow}|{\rm GS}\rangle$ with total spin $S_z^{\rm max} - 1/2 - 1$. Here there are two spin-up electrons and one hole with spin-down in the spin-polarized ground state. The interaction between the two electrons and a hole leads to the formation of trion states. We form a Hamiltonian matrix in the space of three-particle configurations and diagonalize it to obtain trion states. If the energy of the lowest trion state with $S_z^{\rm max} - 1/2 - 1$ is lower than the energy of any of the charged TGQD states $|i\rangle$ with $S_z^{\rm max} - 1/2$, the minority spin electron forms a bound state with the spin-flip exciton, a trion, and the spin-polarized state of a charged TGQD is unstable. The trion binding energy, shown in Fig. 9, is found to be negative for small systems with $N_{\rm edge} \leqslant 8$ and positive for all larger systems studied here. The binding of the trion, i.e., the negative binding energy, is consistent with the complete spin depolarization obtained using TB + HF + CI method for TGQD with $N_{\rm edge} \leqslant 9$ but not observed for $N_{\rm edge} = 11$ (and not observed for $N_{\rm edge} = 10$, not shown here), as shown in Fig. 8. For small systems, a minority spin-up electron triggers spin-flip excitations, which leads to the spin depolarization. With increasing size, the effect of the correlations close to the charge neutrality vanishes. At a critical size, around $N_{\rm edge} = 8$, indicated by an arrow in Fig. 9,

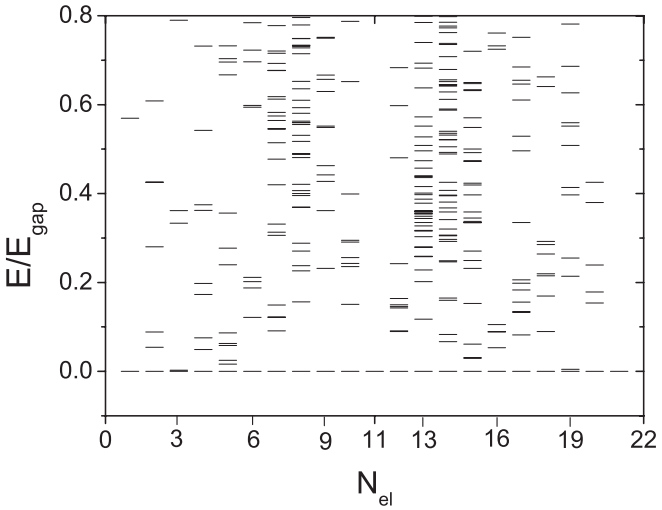

FIG. 10. The low-energy spectra of the many-body states as a function of the number of electrons occupying the degenerate shell for the triangle with $N_{\text{edge}} = 11$ degenerate states. The energies are renormalized by the energy gap corresponding to the half-filled shell, $N_{\text{el}} = 11$ electrons. The large density of states related to the correlation effects observed in Fig. 4 around $N_{\text{edge}} + 1$ electrons shifts to a different filling around $N_{\text{edge}} + 3$ electrons.

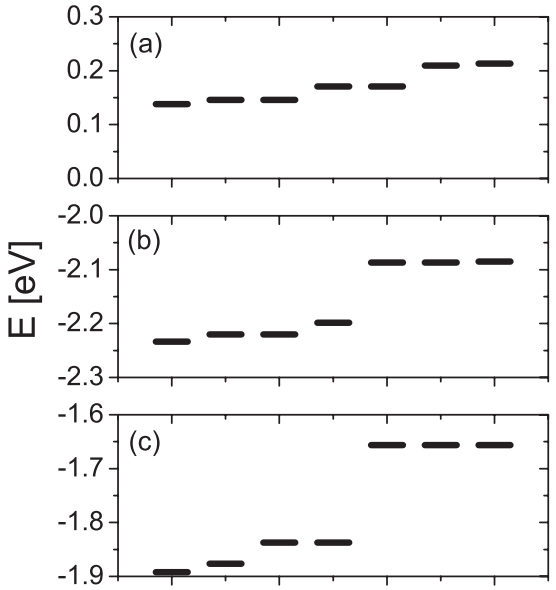

FIG. 11. Hartree-Fock energy levels corresponding to the degenerate shell for calculations with (a) only the on-site term U (Hubbard model), (b) the on-site term U + direct long-range interaction (extended Hubbard model), and (c) all interactions. A separation of three corner states with higher energies is related to direct long-range Coulomb interaction terms.

a quantum phase transition occurs from minimum to maximum total spin.

However, the spin depolarization does not vanish but moves to different filling factors. In Fig. 8 we observe that the minimum spin state for the largest structure computed by the TB + HF + CI method with $N_{\text{edge}} = 11$ occurs for TGQD charged with additional three electrons. We recall that for TGQD with $N_{\text{edge}} = 7$ charged with three additional electrons a formation of a Wigner-like spin-polarized molecule was observed, shown in Fig. 6. In the following, the differences in the behavior of these two systems, $N_{\text{edge}} = 7$ and 11, will be explained based on the analysis of the many-body spectrum of the $N_{\text{edge}} = 11$ system.

Figure 10 shows the many-body energy spectra for different numbers of electrons for $N_{\text{edge}} = 11$ TGQD to be compared with Fig. 4 for the $N_{\text{edge}} = 7$ structure. Energies are renormalized by the energy gap of a half-filled shell, $N_{\text{el}} = 11$ electrons in this case. In contrast to the $N_{\text{edge}} = 7$ structure, energy levels corresponding to $N_{\text{el}} = N_{\text{edge}} + 1$ electrons are sparse, whereas increased low-energy densities of states appear for $N_{\text{el}} = N_{\text{edge}} + 2$ and $N_{\text{el}} = N_{\text{edge}} + 3$ electrons. In this structure, electrons are not as strongly confined as for smaller systems. Therefore, for $N_{\text{el}} = N_{\text{edge}} + 3$ electrons, geometrical effects that lead to the formation of a Wigner-like molecule become less important. Here, correlations dominate, which results in a large low-energy density of states.

IV. DIFFERENT LEVELS OF APPROXIMATIONS ANALYSIS

In this section, we study the role of different interaction terms included in our calculations. The computational procedure is identical to that described in Sec. II. We start from the TB model but in self-consistent HF and CI calculations we include only specific Coulomb matrix elements. We compare results obtained with Hubbard model with only the on-site term, the extended Hubbard model with on-site plus long-range Coulomb interactions, and a model with all direct and exchange terms calculated for up to next-nearest neighbors using Slater orbitals, and all longer-range direct Coulomb interaction terms approximated as $\langle ij|V|ji\rangle = 1/(\kappa|r_i - r_j|)$, written in atomic units, 1a.u. = 27.211 eV, where r_i and r_j are positions of i-th and j-th sites, respectively.

The comparison of HF energy levels for the structure with $N_{\text{edge}} = 7$ is shown in Fig. 11. The on-site U term slightly removes degeneracy of the perfectly flat shell [Fig. 11(a)] and unveils the double valley degeneracy. On the other hand, the direct long-range Coulomb interaction separates three corner states from the rest with a higher energy [Fig. 11(b)], forcing the lifting of one of the doubly degenerate subshells. Finally, the inclusion of exchange and scattering terms causes stronger removal of the degeneracy and changes the order of the four lower-lying states. However, the form of the HF orbitals is not affected significantly (not shown here).

In Fig. 12 we study the influence of different interaction terms on CI results. The phase diagrams obtained within (a) the Hubbard model and (b) the extended Hubbard model show that all electronic phases are almost always fully spin polarized. The ferromagnetic order for the charge-neutral system is properly predicted. For TGQD charged with electrons, only inclusion of all Coulomb matrix elements correctly predicts the effect of the correlations leading to the complete depolarization for $N_{\text{el}} = 8$ and 9. We note that the depolarizations at other filling factors are also observed in Hubbard (at $N_{\text{el}} = 2$) and extended Hubbard calculation (at $N_{\text{el}} = 11$) results.

A more detailed analysis can be done by looking at the energy excitation gaps, which are shown in Fig. 13. For the charge-neutral system, all three methods give comparable

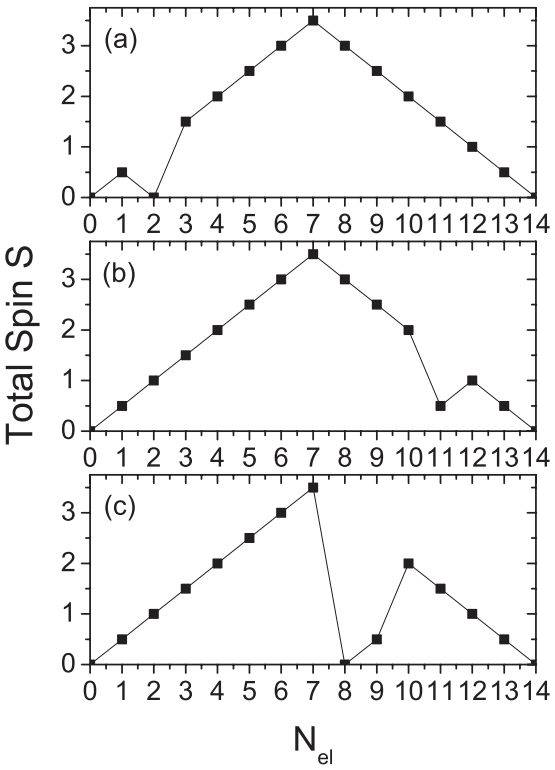

FIG. 12. Spin phase diagrams obtained by use of the CI method with (a) only the on-site term U (Hubbard model), (b) the on-site term U + direct long-range interaction (extended Hubbard model), and (c) all interactions. The ferromagnetic order for the charge-neutral system is properly predicted by all three methods. Correlations leading to the complete depolarization for $N_{el} = N_{edge} + 1$ electrons and $N_{el} = N_{edge} + 2$ electrons are observed only within a full interacting Hamiltonian.

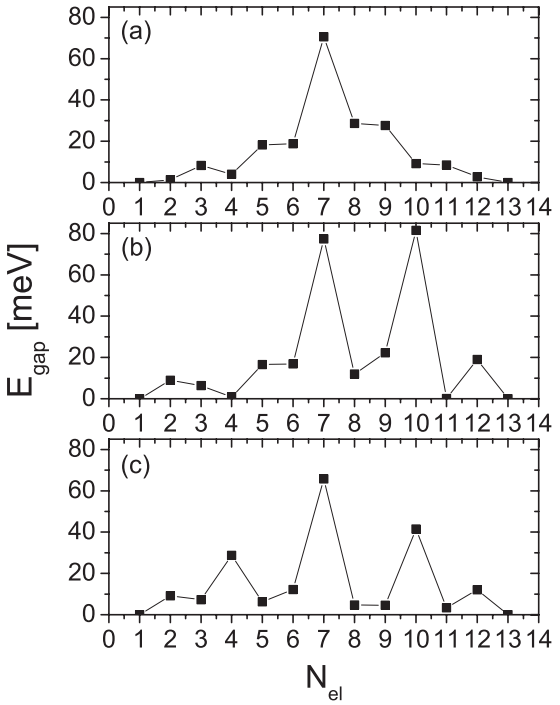

FIG. 13. The excitation gaps corresponding to phase diagrams from Fig. 12 for many-body Hamiltonians with (a) only the on-site term U (Hubbard model), (b) the on-site term U + direct long-range interaction (extended Hubbard model), and (c) all interactions. All three methods give qualitatively similar excitation gaps for the charge-neutral system. A large energy gap for $N_{el} = N_{edge} + 3$ electrons, which is related to geometrical properties of the structure, can be obtained by inclusion of direct long-range interactions. This gap is slightly reduced by inclusion of exchange and scattering terms.

excitation gaps, in agreement with previous results.[42,43,50,51] In the Hubbard model, the energy gap of the doped system is reduced compared to the charge neutrality but without affecting magnetic properties. The inclusion of a direct long-range interaction in Fig. 13(b) induces oscillations of the energy gap. For $N_{el} = N_{edge} + 1$ electrons the energy gap is significantly reduced but the effect is not sufficiently strong to depolarize the system. Further away from half-filling, a large energy gap for models with long-range interactions for $N_{el} = N_{edge} + 3$ appears, corresponding to the formation of a Wigner-like molecule of three spin-polarized electrons in three different corners. The inclusion of exchange and scattering terms slightly reduces the gap but without changing a main effect of Wigner-like molecule formation.

V. CONCLUSIONS AND REMARKS

We have investigated magnetism, correlations, and geometrical effects in TGQDs by use of the TB + HF + CI method. Our many-body Hamiltonian includes all direct long-range terms and exchange and scattering terms up to next-nearest neighbors. We have performed analysis as a function of the filling factor of the degenerate band of edge states for different sizes. Through a full analysis of the many-body energy spectrum of structures consisting of up to 200 atoms, we confirmed the existence of the spin-polarized ground state in agreement with Lieb's theorem. By studying spin exciton binding energies, we also predicted stable magnetization for structures with more than 500 atoms. The complete spin depolarization was observed for one electron added to the charge-neutral TGQD up to a critical size. Above a critical size the maximally spin-polarized charged TGQD was predicted using trion binding energy analysis. We have shown that in small systems, three electrons/holes added to the charge neutrality form the spin-polarized Wigner-like molecule. We relate this fact to geometrical effects and direct long-range interaction terms. For larger systems, geometry becomes less important and for the same filling we observe a spin depolarization as a result of correlations. Finally, we compared the fully interacting model with the Hubbard and extended Hubbard models. While qualitative agreement for the charge-neutral system was observed, the effect of correlations can be described only with the inclusion of all direct long-range, exchange, and scattering terms.

ACKNOWLEDGMENT

The authors thank NSERC, NRC-CNRS CRP, the Canadian Institute for Advanced Research, Institute for Microstructural Sciences, and QuantumWorks for support. P.P. acknowledges financial support from fellowship cofinanced by European

Union within European Social Fund. A.W. acknowledges support from the EU Marie Curie CIG.

APPENDIX

In this Appendix, we calculate density matrix elements $\rho^o_{jl\sigma'}$ between sites j and l for an infinite graphene sheet. The valence band eigenfunctions of the TB Hamiltonian in the nearest-neighbor approximation given by Eq. (2) are

$$\Psi^v_{\mathbf{k}}(\mathbf{r}) = \frac{1}{\sqrt{2N_c}}\left[\sum_{\mathbf{R_A}} e^{i\mathbf{kR_A}}\phi_z(\mathbf{r}-\mathbf{R_A}) + \sum_{\mathbf{R_B}} e^{i\mathbf{kR_B}}e^{-i\mathbf{kb}}e^{-i\theta_{\mathbf{k}}}\phi_z(\mathbf{r}-\mathbf{R_B})\right], \quad \text{(A1)}$$

where $\phi_z(\mathbf{r})$ are p_z orbitals. The positions of the sublattice A and B atoms are given by $\mathbf{R_A} = n\mathbf{a}_1 + m\mathbf{a}_2$ and $\mathbf{R_B} = n\mathbf{a}_1 + m\mathbf{a}_2 + \mathbf{b}$, described by unit vectors of hexagonal lattice defined as $\mathbf{a}_{1,2} = a/2(\pm\sqrt{3},3)$ and $\mathbf{b} = a(0,1)$, a vector between two nearest-neighbors atoms from the same unit cell with a distance $a = 1.42$ Å. N_c is the number of unit cells, and $\exp(i\theta_{\mathbf{k}}) = \frac{f(\mathbf{k})}{|f(\mathbf{k})|}$ with $f(\mathbf{k}) = 1 + e^{i\mathbf{ka}_1} + e^{i\mathbf{ka}_2}$. The density matrix for the graphene layer $\rho^o_{jl\sigma}$ for two sites j and l is defined as

$$\rho^o_{jl\sigma} = \sum_{\mathbf{k}} b_{\mathbf{R}_j}(\mathbf{k}) b_{\mathbf{R}_l}(\mathbf{k}), \quad \text{(A2)}$$

where $b_{\mathbf{R}}$'s are the coefficients of the p_z orbitals given in Eq. (A1). The on-site density matrix element for an arbitrary lattice site j is site and sublattice index independent,

$$\rho^o_{jj\sigma} = \frac{1}{2N_c}\sum_{\mathbf{k}} e^{-i\mathbf{kR}_j}e^{i\mathbf{kR}_j} = \frac{1}{2N_c}\sum_{\mathbf{k}} 1 = \frac{1}{2}, \quad \text{(A3)}$$

where we took into account the fact that the number of occupied states is equal to the number of unit cells in the system. The nearest-neighbors density matrix elements for two atoms from the same unit cell corresponds to $\mathbf{R}_l - \mathbf{R}_j = \mathbf{b}$ and can be calculated using

$$\rho^o_{jl\sigma} = \frac{1}{2N_c}\sum_{\mathbf{k}} e^{-i\mathbf{kR}_j}e^{i\mathbf{kR}_l}e^{-i\mathbf{kb}}e^{-i\theta_{\mathbf{k}}} = \frac{1}{2N_c}\sum_{\mathbf{k}} e^{-i\theta_{\mathbf{k}}} \simeq 0.262,$$

where the summation over occupied valence states is carried out numerically. We obtained the same value for two other nearest neighbors. The same results can also be obtained by diagonalizing a sufficiently large hexagonal graphene quantum dot and by computing the density matrix elements for two nearest neighbors in the vicinity of the center of the structure. We have also calculated next-nearest neighbors density matrix elements, obtaining negligibly small values.

[1] K. S. Novoselov, A. K. Geim, S. V. Morozov, D. Jiang, Y. Zhang, S. V. Dubonos, I. V. Grigorieva, and A. A. Firsov, Science **306**, 666 (2004).

[2] K. S. Novoselov, A. K. Geim, S. V. Morozov, D. Jiang, M. I. Katsnelson, I. V. Grigorieva, S. V. Dubonos, and A. A. Firsov, Nature **438**, 197 (2005).

[3] Y. B. Zhang, Y. W. Tan, H. L. Stormer, and P. Kim, Nature **438**, 201 (2005).

[4] Y. W. Son, M. L. Cohen, and S. G. Louie, Phys. Rev. Lett. **97**, 216803 (2006).

[5] M. L. Sadowski, G. Martinez, M. Potemski, C. Berger, and W. A. de Heer, Phys. Rev. Lett. **97**, 266405 (2006).

[6] A. K. Geim and K. S. Novoselov, Nat. Mater. **6**, 183 (2007).

[7] A. Rycerz, J. Tworzydlo, and C. W. Beenakker, Nat. Phys. **3**, 172 (2007).

[8] F. Xia, T. Mueller, Y.-M. Lin, A. Valdes-Garcia, and P. Avouris, Nat. Nanotechnol. **4**, 839 (2009).

[9] T. Mueller, F. Xia, and P. Avouris, Nat. Photon. **4**, 297 (2010).

[10] A. H. C. Neto, F. Guinea, N. M. R. Peres, K. S. Novoselov, and A. K. Geim, Rev. Mod. Phys. **81**, 109 (2009).

[11] A. H. Rozhkov, G. Giavaras, Y. P. Bliokh, V. Freilikher, and F. Nori, Phys. Rep. **503**, 77 (2011).

[12] A. H. Abergel, G. Apalkov, Y. P. Berashevich, V. Ziegler, and F. Chakraborty, Adv. Phys. **59**, 261 (2010).

[13] X. Li, X. Wang, L. Zhang, S. Lee, and H. Dai, Science **319**, 1229 (2008).

[14] L. A. Ponomarenko, F. Schedin, M. I. Katsnelson, R. Yang, E. W. Hill, K. S. Novoselov, and A. K. Geim, Science **320**, 356 (2008).

[15] L. Ci, Z. Xu, L. Wang, W. Gao, F. Ding, K. F. Kelly, B. I. Yakobson, and P. M. Ajayan, Nano Res. **1**, 116 (2008).

[16] Y. You, Z. Ni, T. Yu, and Z. Shena, Appl. Phys. Lett. **93**, 163112 (2008).

[17] S. Schnez, F. Molitor, C. Stampfer, J. Güttinger, I. Shorubalko, T. Ihn, and K. Ensslin, Appl. Phys. Lett. **94**, 012107 (2009).

[18] K. A. Ritter and J. W. Lyding, Nat. Mater. **8**, 235 (2009).

[19] X. Jia, M. Hofmann, V. Meunier, B. G. Sumpter, J. Campos-Delgado, J. M. Romo-Herrera, H. Son, Y.-P. Hsieh, A. Reina, J. Kong, M. Terrones, and M. S. Dresselhaus, Science **323**, 1701 (2009).

[20] L. C. Campos, V. R. Manfrinato, J. D. Sanchez-Yamagishi, J. Kong, and P. Jarillo-Herrero, Nano Lett. **9**, 2600 (2009).

[21] S. Neubeck, Y. M. You, Z. H. Ni, P. Blake, Z. X. Shen, A. K. Geim, and K. S. Novoselov, Appl. Phys. Lett. **97**, 053110 (2010).

[22] L. P. Biró and Ph. Lambin, Carbon **48**, 2677 (2010).

[23] E. Cruz-Silva, A. R. Botello-Mendez, Z. M. Barnett, X. Jia, M. S. Dresselhaus, H. Terrones, M. Terrones, B. G. Sumpter, and V. Meunier, Phys. Rev. Lett. **105**, 045501 (2010).

[24] R. Yang, L. Zhang, Y. Wang, Z. Shi, D. Shi, H. Gao, E. Wang, and G. Zhang, Adv. Mater. **22**, 4014 (2010).

[25] B. Krauss, P. Nemes-Incze, V. Skakalova, L. P. Biró, K. von Klitzing, and J. H. Smet, Nano Lett. **10**, 4544 (2010).

[26] L. Zhi and K. Müllen, J. Mater. Chem. **18**, 1472 (2008).

[27] M. Treier, C. A. Pignedoli, T. Laino, R. Rieger, K. Müllen, D. Passerone, and R. Fasel, Nat. Chem. **3**, 61 (2010).

[28]M. L. Mueller, X. Yan, J. A. McGuire, and L. Li, Nano Lett. **10**, 2679 (2010).
[29]Y. Morita, S. Suzuki, K. Sato, and T. Takui, Nat. Chem. **3**, 197 (2011).
[30]J. Lu, P. S. E. Yeo, C. K. Gan, P. Wu, and K. P. Loh, Nat. Nanotechnol. **6**, 247 (2011).
[31]A. K. Singh and B. I. Yakobson, Nano Lett. **9**, 1540 (2009).
[32]V. Tozzini and V. Pellegrini, Phys. Rev. B **81**, 113404 (2010).
[33]H. Xiang, E. Kan, S.-H. Wei, M.-H. Whangbo, and J. Yang, Nano Lett. **9**, 4025 (2009).
[34]M. J. Schmidt and D. Loss, Phys. Rev. B **82**, 085422 (2010).
[35]T. Yamamoto, T. Noguchi, and K. Watanabe, Phys. Rev. B **74**, 121409 (2006).
[36]Z. Z. Zhang, K. Chang, and F. M. Peeters, Phys. Rev. B **77**, 235411 (2008).
[37]A. D. Güçlü, P. Potasz, and P. Hawrylak, Phys. Rev. B **82**, 155445 (2010).
[38]K. Nakada, M. Fujita, G. Dresselhaus, and M. S. Dresselhaus, Phys. Rev. B **54**, 17954 (1996).
[39]M. Fujita, K. Wakabayashi, K. Nakada, and K. Kusakabe, J. Phys. Soc. Jpn. **65**, 1920 (1996).
[40]Y. Son, M. L. Cohen, and S. G. Louie, Nature **444**, 347 (2006).
[41]M. Ezawa, Phys. Rev. B **73**, 045432 (2006).
[42]M. Ezawa, Phys. Rev. B **76**, 245415 (2007).
[43]J. Fernandez-Rossier and J. J. Palacios, Phys. Rev. Lett. **99**, 177204 (2007).
[44]J. Akola, H. P. Heiskanen, and M. Manninen, Phys. Rev. B **77**, 193410 (2008).
[45]W. L. Wang, O. V. Yazyev, S. Meng, and E. Kaxiras, Phys. Rev. Lett. **102**, 157201 (2009).
[46]P. Potasz, A. D. Güçlü, and P. Hawrylak, Phys. Rev. B **81**, 033403 (2010).
[47]Y. Niimi, T. Matsui, H. Kambara, K. Tagami, M. Tsukada, and H. Fukuyama, Appl. Surf. Sci. **241**, 43 (2005).
[48]Y. Kobayashi, K.-I. Fukui, T. Enoki, K. Kusakabe, and Y. Kaburagi, Phys. Rev. B **71**, 193406 (2005).
[49]C. Tao, L. Jiao, O. V. Yazyev, Y.-C. Chen, J. Feng, X. Zhang, R. B. Capaz, J. M. Tour, A. Zettl, S. G. Louie, H. Dai, and M. F. Crommie, Nat. Phys. **7**, 616 (2011).
[50]W. L. Wang, S. Meng, and E. Kaxiras, Nano Lett. **8**, 241 (2008).
[51]A. D. Güçlü, P. Potasz, O. Voznyy, M. Korkusinski, and P. Hawrylak, Phys. Rev. Lett. **103**, 246805 (2009).
[52]M. Ezawa, Phys. Rev. B **77**, 155411 (2008).
[53]M. R. Philpott, F. Cimpoesu, and Y. Kawazoe, Chem. Phys. **354**, 1 (2008).
[54]H. P. Heiskanen and M. Manninen, J. Akola, New J. Phys. **10**, 103015 (2008).
[55]D. P. Kosimov, A. A. Dzhurakhalov, and F. M. Peeters, Phys. Rev. B **81**, 195414 (2010).
[56]M. Ezawa, Phys. Rev. B **81**, 201402 (2010).
[57]M. Ezawa, Physica E **42**, 703 (2010).
[58]O. Voznyy, A. D. Güçlü, P. Potasz, and P. Hawrylak, Phys. Rev. B **83**, 165417 (2011).
[59]H. Sahin, R. T. Senger, and S. Ciraci, J. Appl. Phys. **108**, 074301 (2010).
[60]I. Romanovsky, C. Yannouleas, and U. Landman, Phys. Rev. B **83**, 045421 (2011).
[61]Y. Xi, M. Zhao, X. Wang, S. Li, X. He, Z. Wang, and H. Bu, J. Phys. Chem. C **113**, 12637 (2009).
[62]M. Kinza, J. Ortloff, and C. Honerkamp, Phys. Rev. B **82**, 155430 (2010).
[63]M. Zarenia, A. Chaves, G. A. Farias, and F. M. Peeters, Phys. Rev. B **84**, 245403 (2011).
[64]Q. Q. Dai, Y. F. Zhu, and Q. Jiang, Phys. Chem. Chem. Phys. **14**, 1253 (2012).
[65]E. H. Lieb, Phys. Rev. Lett. **62**, 1201 (1989).
[66]P. R. Wallace, Phys. Rev. **71**, 622 (1947).
[67]B. J. Ransil, Rev. Mod. Phys. **32**, 245 (1960).
[68]P. Potasz, A. D. Güçlü, and P. Hawrylak, Phys. Rev. B **82**, 075425 (2010).
[69]S. Reich, J. Maultzsch, C. Thomsen, and P. Ordejón, Phys. Rev. B **66**, 035412 (2002).
[70]A. Bostwick, T. Ohta, J. L. McChesney, T. Seyller, K. Horn, and E. Rotenberg, Solid State Commun. **143**, 63 (2007).
[71]R. S. Deacon, K.-C. Chuang, R. J. Nicholas, K. S. Novoselov, and A. K. Geim, Phys. Rev. B **76**, 081406(R) (2007).
[72]B. Wunsch, T. Stauber, and F. Guinea, Phys. Rev. B **77**, 035316 (2008).
[73]I. Romanovsky, C. Yannouleas, and U. Landman, Phys. Rev. B **79**, 075311 (2009).
[74]P. Hawrylak, A. Wojs, and J. A. Brum, Phys. Rev. B **55**, 11397 (1996).